Journal of Hydrology 600 (2021) 126522

Contents lists available at ScienceDirect

Journal of Hydrology

journal homepage: www.elsevier.com/locate/jhydrol

Research papers

Mapping dynamic non-perennial stream networks using high-resolution distributed hydrologic simulation: A case study in the upper blue river basin

Shang Gao [a,*], Mengye Chen [a], Zhi Li [a], Stephen Cook [b], Daniel Allen [b], Thomas Neeson [c], Titantian Yang [a], Teshome Yami [a], Yang Hong [a,*]

[a] School of Civil Engineering and Environmental Science, University of Oklahoma, Norman, OK, USA
[b] Department of Biology, University of Oklahoma, Norman, OK, USA
[c] Department of Geography & Environmental Sustainability, University of Oklahoma, Norman, OK, USA

ARTICLE INFO

This manuscript was handled by Sally Elizabeth Thompson, Editor-in-Chief

Keywords:
Stream dynamics
Non-perennial tributaries
Blue river basin
Low flow condition
Distributed hydrological modeling
LANDSAT imagery
In-situ state logger

ABSTRACT

More than half of all streams globally are non-perennial, and thus dynamic due to their expanding and retracting nature. Field mapping in conjunction with observational data from gauges and/or in-situ loggers is a typical approach for studying non-perennial stream dynamics, but these approaches underrepresent their spatiotemporal variability. High-resolution distributed hydrological modeling promises to bridge this gap, thanks to advances in model physics, remote sensing, and computational power. As the first step towards this goal, we investigate the capability of distributed hydrologic modeling to capture stream dynamics in Upper Blue River Basin, OK. Coupled Routing and Excess STorage (CREST), a distributed hydrological model, is used to simulate spatio-temporally varied streamflow at 10-meter spatial resolution and daily time steps. USGS stream gauge data and in-situ state logger data are used to calibrate and validate the simulation at the watershed outlet and small headwater tributaries, respectively. Dynamic Surface Water Estimate (DSWE), a LANDSAT product is also compared with simulated water presence in high-order streams. Results show that the CREST model can capture low-moderate streamflow values at the watershed outlet with a log-NSE value over 0.7 in the validation period, while underestimating high flow values due to the daily time step. Also, the calibrated model can accurately estimate wet/dry status as monitored by in-situ state loggers in nine headwater catchments. The dynamic stream networks are mapped over 2510 stream segments using the CREST simulation. Non-perennial streams are the most dynamic in small headwater tributaries (contributing area <2 km^2) and high-order streams are sustained by perennial flow. As hydrologic interpretation of the stream dynamics, the interannual and seasonal variability in rainfall and evapotranspiration is well reflected by the water occurrence in streams. Across various catchments, a consistent threshold behavior is found between drainage density and unit discharge, indicating the control of runoff generation on the flowing stream networks. The mapping also identifies differences in stream dynamics caused by heterogeneities in land cover and soil properties. Given the prevalence of dynamical streams worldwide, our analysis illustrates the potential for mapping them using distributed hydrologic models.

1. Introduction

Out of all of the Earth's streams, non-perennial streams (those that do not continuously flow, Busch et al., 2020) comprise about half of the total stream length (Datry et al., 2014). These streams often reside in headwaters and extend/retract seasonally and during storm events (e.g., Jensen et al., 2017; Shaw, 2016). The frequency, timing, and duration of drying in non-perennial streams are particularly important for river ecosystems at multiple spatiotemporal scales (Allen et al., 2020; Larned et al., 2010; Walker et al., 1995). In spite of their ecological and hydrological significance, the actively flowing stream networks and their spatiotemporal dynamics have received relatively little attention until recent years. Many field surveys have been conducted to investigate stream dynamics at seasonal and storm event scales (Durighetto et al., 2020; Godsey and Kirchner, 2014; Goulsbra et al., 2014; Jensen et al., 2019; Lovill et al., 2018; Meerveld et al., 2019; Peirce and Lindsay,

* Corresponding authors.
E-mail addresses: shang.gao@ou.edu (S. Gao), yanghong@ou.edu (Y. Hong).

https://doi.org/10.1016/j.jhydrol.2021.126522
Received 16 September 2020; Received in revised form 27 May 2021; Accepted 31 May 2021
Available online 3 June 2021
0022-1694/Published by Elsevier B.V.

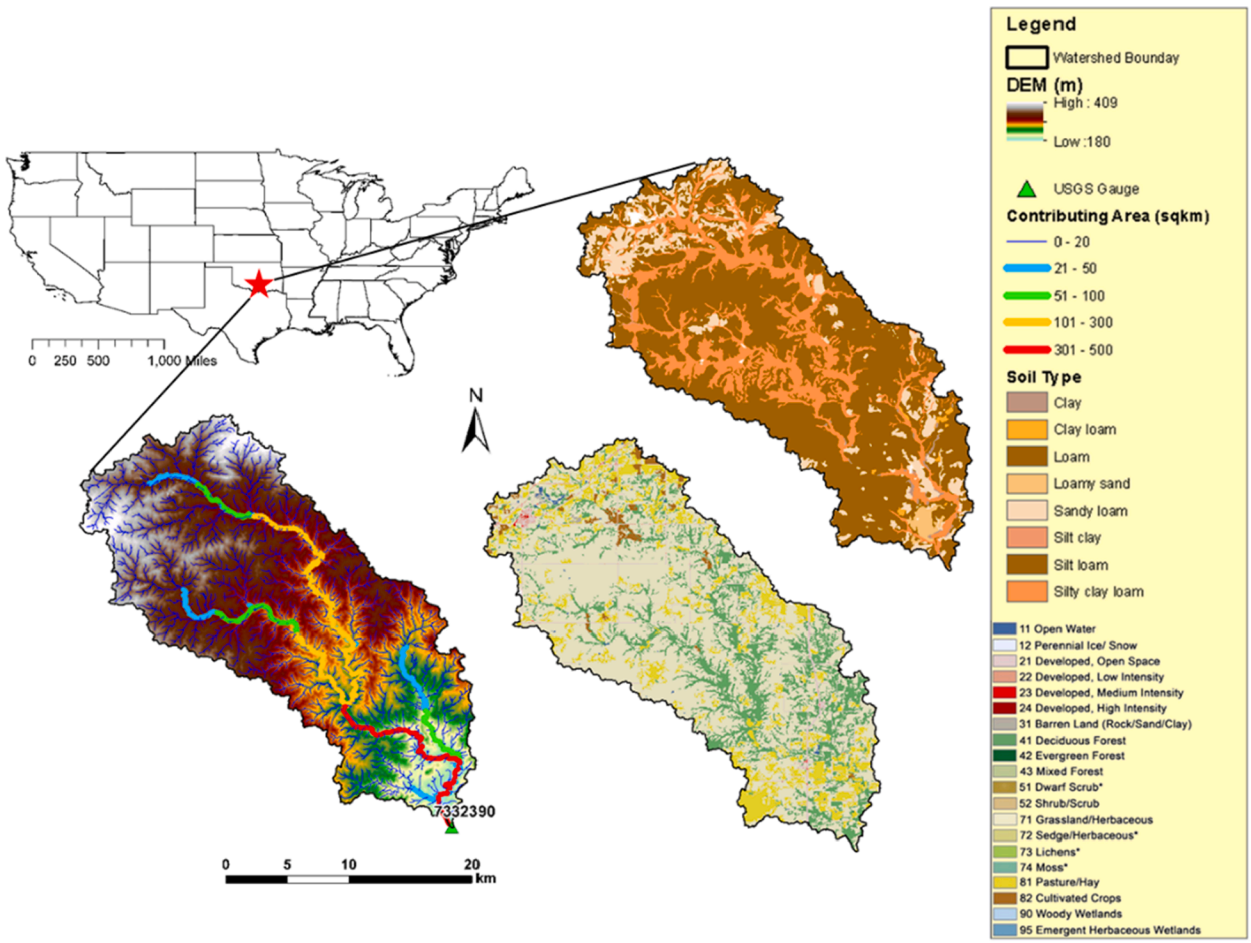

Fig. 1. Maps of the relative location in US, digital elevation model with stream networks, land cover, soil types of the upper blue river basin (UBRB). (For interpretation of the references to color in this figure legend, the reader is referred to the web version of this article.)

2015; Shaw et al., 2017; Whiting and Godsey, 2016; Zimmer and McGlynn, 2017). A common finding from these studies is that climate variabilities cause a major proportion the global stream networks to be dynamic. The non-perennial streams in headwaters play a major role in shaping the stream dynamics (Bishop et al., 2008), and thus need to be characterized with accuracy and spatiotemporal granularity.

Compared with perennial streams, it is more challenging to characterize the non-perennial streams because of the distinct hydro-meteorologic settings, e.g. rainfall and evapotranspiration irregularity, soil and land cover heterogeneities (Niedda and Pirastru, 2014; Peleg et al., 2015). Most importantly, the sources of hydrological data are limited in coverage and spatial density. The primary source has been gauging data, but gauge stations are often spatially sparse and on perennial rivers close to urban areas (Benstead and Leigh, 2012; Datry, 2012) rather than in headwaters where non-perennial streams are located (De Girolamo et al., 2015; Eng et al., 2016). In addition, various loggers can be deployed spatially to measure electrical conductivity (Chapin et al., 2014), water temperature (Constantz et al., 2001), and water level and/or the presence-absence of water (Bhamjee and Lindsay, 2011; Vander Vorste et al., 2016). Time series data from the loggers can be used to track the movement of wetting and drying fronts (Bhamjee and Lindsay, 2011) and the persistence of surface waters in different reaches (Vander Vorste et al., 2016).

Remote sensing is an emerging way to monitor non-perennial streams. Various remote sensing techniques have been used to measure proxies for discharge (e.g., river height or width) from which to estimate flow regimes. Examples of these techniques are air- and space-borne measurements of surface velocity; radar altimeters to measure surface-water elevations; and measurements of wetted areas and bank heights to estimate flow volumes (Costa et al., 2013; Gleason and Smith, 2014; Puckridge et al., 2000). However, most remote sensing techniques are best suited for large rivers and have limited utility for small headwater streams due to low spatial resolution and dense vegetation cover (Costigan et al., 2017). Out of the all remotely sensed data, satellite imagery has relatively high spatial resolution with vast spatial extent but low temporal frequency, which is insufficient for capturing the stream intermittency that can be temporally dynamic (Hamada et al., 2016).

When monitoring approaches have only limited data for a location of interest at some discontinuous time steps, modeling approaches can provide high spatiotemporal granularity and predict/simulate scenarios in response to changing environmental conditions, such as global change and water extraction for human uses. The key to successful simulation of non-perennial streams firstly depends on the capability of model structure to represent transition from low to zero flow regime, or the discontinuities in the flow regime (Azarnivand et al., 2020a; Camporese et al., 2014, 2019). Also, the water balance should be calculated integrating various catchment storges, i.e. streams, soils and groundwater (Azarnivand et al., 2020b). Lumped models are explored in many studies (e.g., Cipriani et al., 2014; Ivkovic et al., 2014; Ye et al., 1997) because of the easy of application, low data requirement, few parameters, and good performance at the catchment outlet. For example, the widely-used Soil Water Assessment Tool (SWAT, Gassman et al., 2007) accounts for precipitation, evapotranspiration, surface runoff, infiltration, lateral flow, and percolation and has been successful in modeling and also projecting flow intermittency under natural, current, and future conditions (e.g., Chahinian et al., 2011; Tzoraki et al., 2016; Brown

et al., 2015). In comparison, distributed hydrological modeling receives spatially refined geographical data, meteorologic forcing and tracks or outputs models fluxes (streamflow, infiltration, evapotranspiration) and states (soil moisture, groundwater levels). In recent studies on non-perennial streams, increasing attention is given to distributed models that integrate surface and sub-surface water by solving multiple nonlinear dynamics (Fatichi et al., 2016). For example, the CATHY (Catchment Hydrology) model has been applied in intermittent or ephemeral catchments to investigate afforestation (Azarnivand et al., 2020a), water balance complexities due to heterogeneous land use (Dean et al., 2016), and hydrologic response to rainfall frequency (Azarnivand et al., 2020b). Also, the model MIKE SHE was used to study water and salt dynamics of intermittent catchments (Daneshmand et al., 2019, 2020). As commonly pointed out in these studies, distributed models are well-suited for natural catchments (Fatichi et al., 2016) as the heterogeneous, dynamic water movements across surface and sub-surface layers are dealt with in an integrated continuum.

However, these few modeling studies of non-perennial streams/tributaries mostly focus on small-sized headwater catchments. The limited spatial scale does not fully cover the stream dynamics across various stream orders. Meanwhile, previous studies on stream dynamics mostly reply on monitoring approaches via fixed gauges, loggers, and field surveys, which is limited by the logistical challenges, spatial density, temporal frequency of the collected data (e.g., Bhamjee and Lindsay, 2011; Godsey and Kirchner, 2014; Jensen et al., 2019; Peirce and Lindsay, 2015). To bridge this gap, we use high-resolution process-based distributed hydrologic modeling over a relatively large catchment to provide streamflow estimates of high spatial density and temporal frequency as the base of mapping stream dynamics. The combination of high spatial resolution and large scale enables a comprehensive view of numerous small non-perennial headwater tributaries as well as the high-order perennial streams. Moreover, stream gauge and state logger data are used for calibrating and validating model outputs to improve model performance at various stream orders. The feasibility of satellite images in detecting stream dynamics is also explored.

The overarching goal is to provide a-priori estimates and hydrologic interpretations of the stream dynamics across non-perennial and perennial tributaries using high-resolution distributed modeling. The study aims to answer the following research questions: 1) As indicators of stream dynamics, can the model simulation capture flow values in high-order large streams, and wet/dry status in low-order non-perennial streams? 2) In spite of their inherent limitations, whether and how can satellite imagery products and in-situ state loggers be utilized in hydrologic modeling as calibration/validation sources? 3) How do the actively flowing networks vary in space and time in response to seasonal wetting and drying?

The paper is organized as follows. Section 2 describes the study area, data used in this study, model configuration, and methodology. Section 3 presents the results of hydrologic performance, comparison of CREST and satellite imagery, validation using in-situ state loggers, mapping of dynamic streams, as well as discussion on the results. Section 4 concludes the study and proposes future directions.

2. Methodology

2.1. Study area

The study area is the headwaters of the Blue River Basin, or the Upper Blue River Basin (hereafter, UBRB) located in Southeastern Oklahoma with a drainage area of 483 km^2. Typical of a continental climate, the region experiences occasional extremes of temperature and precipitation. Severe weather including tornadoes and thunderstorms occur in the region as a result of interactions between cold and warm air masses. The mean annual precipitation, temperature, and snow percentages are 1116 mm, 16.4 °C, and 8.2% from 1980 to 2020 according to National Climate Data Center's archive of global historical weather and climate data (https://www.ncdc.noaa.gov/cdo-web/search). The blue river basin features a dry period from May to September, and a wet period in March and April in terms of runoff (Li et al., 2012). The potential evapotranspiration in the dry period is higher than in the wet period by a factor of 3 (Li et al., 2012). Also, storms have higher intensity but shorter durations in the dry period than in the wet period, but the total storm depths are comparable in the two periods (Li et al., 2012; Tian et al., 2012). As shown in Fig. 1, the dominant land cover is grassland, followed by pasture/hay and deciduous forest, according to National Land Cover Database (https://www.mrlc.gov/data/nlcd-2011-land-cover-conus-0). The dominant soil types are loam and silty clay loam according to Soil Survey Geographic Database (https://data.nal.usda.gov/dataset/soil-survey-geographic-database-ssurgo). The watershed is slightly hilly with elevation ranging from 180 to 409 m above sea level, with an average of 340 m. The baseflow in UBRB is sustained by discharge from the Arbuckle Simpson aquifer. During wet years, the main stem of UBRB has been reported to be perennial all the way to its headwater (Smith et al., 2004).

2.2. Crest model

2.2.1. Model overview

One young family of models called the Coupled Routing and Excess Storage (CREST) was initially developed in 2010 (Wang et al., 2011) with a series of improvements later made on model physics, parameter, and software (Xue et al., 2013; Zhang et al., 2015). CREST is a distributed hydrological model resolving spatiotemporal water and energy fluxes on a regular grid with user-defined resolution. The core components of the CREST model include runoff generation, evapotranspiration, surface routing, and sub-surface routing, which enable a three-dimensional representation of water fluxes. In CREST model, precipitation is first intercepted by canopy layer; infiltration and runoff are then partitioned via the variable infiltration curve concept (Liang et al., 1994; Zhao, 1995). While surface and subsurface water was routed using the linear reservoir equations (Nash, 1957) or 1-D kinematic wave approximation of the de Saint Venant Equation (Singh, 1997), water in excess storages, including interception by the vegetation canopy and subsurface storages in the soil layer, are subject to redistribution back to the atmosphere via evapotranspiration. The water balance and grid-based routing schemes are fully coupled at each time step to represent interactions between atmospheric land surface and subsurface water. In terms of parameterization, CREST enables the use of gridded model parameter in regions where estimation of these values from remote sensing data is possible. Vergara et al., (2016) have developed a-prior distributed CREST parameter sets for the Contiguous United States, which is adopted as initial parameter set for this study. A brief description of CREST model parameters is provided in the Appendix. CREST includes automatic calibration modules, i.e. the shuffled complex evolution (Duan et al., 1992) and Differential Evolution Adaptive Metropolis (DREAM, Vrugt et al., 2009). Another strength of CREST is the compatibility with multiple datasets of remotely sensed meteorological forcing. Furthermore, CREST supports gridded output of model states and fluxes like streamflow, soil moisture, surface runoff, and subsurface runoff.

2.3. Data

2.3.1. Forcing and geographic data

The high-resolution (10 m) Digital-Elevation-Model (DEM) is obtained from USGS Earth Explorer (https://earthexplorer.usgs.gov/) and serves as the base for building CREST model. Previous studies identified the lack of spatial characterization of hydro-meteorologic and geographic conditions as a major challenge in modeling intermittent streams (Costelloe et al., 2005). Therefore, the forcing data and model parameters should sufficiently represent the full range of spatial variability of hydro-meteorologic conditions in the basin. For precipitation

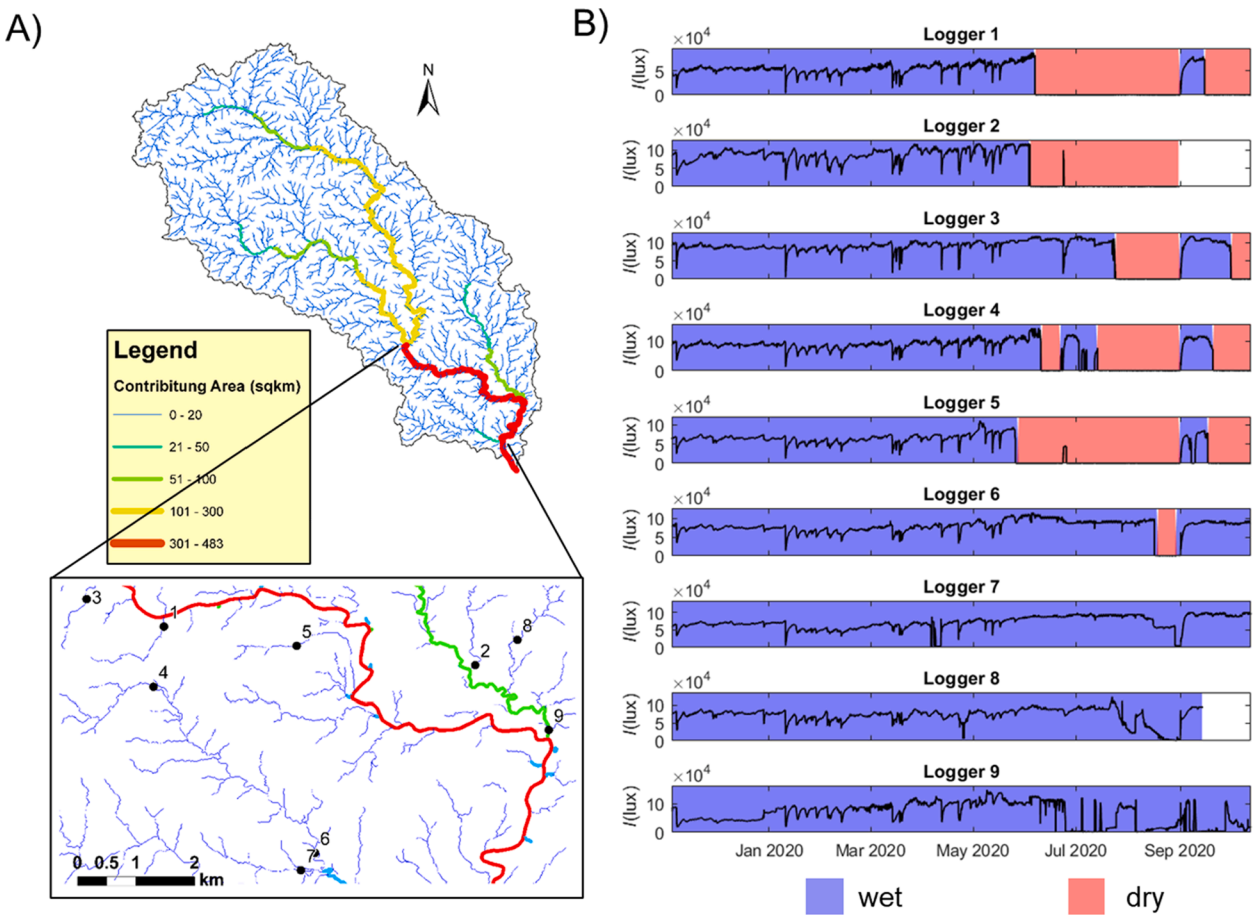

Fig. 2. A) Locations of in-situ state loggers signified by the black round markers and B) the raw conductivity time series measured as light intensity *I* (lux) along with the processed wet/dry states; blank area means no data.

forcing, we used Multi-Radar-Multi-Sensor (MRMS) 1-hour gauge bias-corrected radar precipitation accumulations (Q3GC_SHSR_1H). Q3GC_SHSR_1H is the CoCoRaHS rain-gauge-corrected 1- hour radar QPE accumulation using a three steps method, which has the temporal resolution of 1 h and 1 km^2 spatial resolution (Zhang et al., 2016). The potential evapotranspiration (PET) data used in this study were from United States Geological Survey (USGS) Famine Early Warning Systems Network (FEWS NET, https://earlywarning.usgs.gov/fews). The daily 1 by 1 arc-degree PET data were calculated from the Global Data Assimilation System (GDAS) using the Penman-Monteith method (Verdin et al., 2005). One U.S. Geological Survey (USGS) stream gauge (USGS 07332390) near the downstream outlet of UBRB, were selected to validate and calibrate the hydrological modeling (Fig. 1).

2.3.2. *Dynamic water surface estimate (DSWE)*

The Landsat mission, the Landsat Archive, and on-going Landsat/Sentinel data have enabled great progress in improving long-term observation of inundation at continental and global scales (Pekel et al., 2016). The newly released products by USGS, Dynamic Surface Water Estimate (DSWE), has furthered the ability of this dataset to detect inundation at subpixel level (Jones, 2019). For DSWE product generation, each cloud-, cloud shadow-, and snow-free pixel in a given scene is tested for the presence of standing surface water and classified into either "not water" (NW) or separate "open water" (OW) and "partial surface water" (OSW) classes (Jones, 2019). Specifically, a cell is classified as partially inundated if 20% of its area is covered by water, suggesting detectability of a stream with water 6-meter wide in a 30-meter DSWE cell (Jones, 2019). Therefore, in this study, we explore the potential of DSWE as a validation source for a part of the stream networks with the bank width over 5 m. We conduct field visits along the main stem of UBRB and determine that streams with contributing area over 100 km^2 are targets for comparison with CREST simulation. Below this threshold, the streams get narrower than 5 m and are considered beyond the detectability of DSWE. The raw DSWE data were obtained from USGS Earth Explorer via https://earthexplorer.usgs.gov/. We treat both OW and OSW classes as inundated pixels when compared with the CREST simulation. The comparison is based on DSWE data on 44 selected days when cloud coverage was <10%.

Unlike the common usage of inundation maps to validate hydraulic simulation, DSWE is used here to compare with hydrologic simulation, which only outputs 1-D streamflow rather than 2-D inundation extent or water depth. Therefore, simulation (CREST) and observation (DSWE) are only compared over a series of 10-meter channel cells (with contributing area over 100 km^2). In addition, several preprocessing steps on the raw DSWE dataset are explored, as detailed in the Appendix. The DSWE data are downscaled from 30-meter to 10-meter resolution based on 'nearest neighbor', prior to comparison with the CREST simulation.

2.3.3. *In-situ logger data*

For the small headwater tributaries, we monitored wet/dry status at 9 sites in UBRB using modified Onset HOBO Pendant© loggers that measured stream temperature and conductivity at 30-minute intervals (STIC loggers, Chapin et al., 2014). Conductivity provides a reliable means to estimate drying status by displaying a range of higher values when wet and lower or zero signal when dry. At each stream, we deployed 5 loggers for redundancy in protective PVC housing at different points along a reach by securing them to the streambed using

Table 1
List of statistical metrics used in this study.

Statistic Metrics		Equation	Value Range	Perfect Value	Unit
Evaluation Using USGS Streamflow Observation	Correlation coefficient (CC)	$CC = \frac{\sum_{n=1}^{N}\left(S_n-\overline{S}\right)\left(O_n-\overline{O}\right)}{\sqrt{\sum_{n=1}^{N}\left(S_n-\overline{S}\right)^2}\sqrt{\sum_{n=1}^{N}\left(O_n-\overline{O}\right)^2}}$	$-\infty$, 1	1	N/A
	Relative bias (RB)	$RB = \frac{1}{N}\sum_{n=1}^{N}\frac{S_n-O_n}{O_n}\times 100$	$-\infty$, $+\infty$	0	%
	Log Nash-Sutcliffe coefficient efficiency (log-NSE)	$LogNSE = 1-\frac{\sum_{n=1}^{N}\left(\log(S_n)-\log(O_n)\right)^2}{\sum_{n=1}^{N}\left(\log(O_n)-\log(\overline{(O)})\right)^2}$	$-\infty$, 1	1	N/A
Evaluation Using DSWE and In-situ Loggers	Precision	$Precision = \frac{TP}{TP+FP}$	0, 1	1	N/A
	Recall	$Recall = \frac{TP}{TP+FN}$	0, 1	1	N/A
	F1	$F1 = \frac{2\times Precision\times Recall}{Precision+Recall}$	0, 1	1	N/A
	FalseAlarm Ratio	$FAR = \frac{FP}{FP+TP}$	0, 1	0	N/A

* Variables: n and N are index and total number of samples; S represents simulated flow rate from CREST while O is the observed flow rate from USGS stream gauges. The $\overline{\ }$ sign means the averaging operator. TP means number of true positives; FP means number of false positives; FN means number of false negatives, and TN means number of true negatives.

embedded rebar and zipties. As shown in Fig. 2A, nine monitored reaches drain various contributing areas (from 0.7 to 68 km^2) and belong to different tributaries. This arrangement spanned a range in hydrology and was designed to capture various wetting/drying patterns of streams within the watershed. We deployed loggers for one year from November 2019 to 2020 to ensure measurements included both rainy and dry seasons.

We inferred drying state changes of the loggers using a nonparametric change point analysis (nCPA) of the variation (as the standard deviation) in conductivity measurements over each day of the deployment (Matteson and James, 2014). This eliminated the need for human interpretation of a large range of conductivity values, and standardized signal interpretation across all loggers as daily variation was consistently higher during wet days compared to dry days. We retained estimated change points between wet and dry transition periods (permuted p-value < 0.1), and time increments between change points were assigned either wet (1) or dry (0) status based on the mean conductivity of that increment. This allowed us to estimate drying status of each logger at a 1-day temporal resolution. The nCPA for each logger time-series was run with the ecp package (James and Matteson, 2013) using the divisive hierarchical estimation algorithm with 999 permutations. From the five loggers at each site, the one with the most complete record (least null values) is chosen to represent the site. Fig. 2B shows the time series of conductivity and processed wet/dry status. It can be found that the signal processing can reasonably distinguish transitions between wet and dry status at all nine sites.

2.4. Crest model setup

The CREST model for UBRB is set up over 10-meter grids at daily time steps. One reason for using daily time steps is to offset the computational cost due to the high spatial resolution, long simulation period, and need for calibration. In addition, the future application of the stream dynamics estimates, which are to be linked with ecological/biological variables, determines that the most relevant temporal resolution is also daily. To this end, the hourly MRMS radar data is aggregated to a daily amount. The available MRMS Q3GC_SHSR_1H products span 06/01/2015 to 10/13/2020, which confines the simulation period of this study.

Two calibrations are conducted using the downstream USGS stream gauge data and in-situ logger data, respectively. The a-priori distributed parameter sets are adopted as the default, initial values for the calibration. When calibrating gridded parameters in CREST, a multiplication factor on the parameter matrix is varied and calibrated in each iteration, which retains the spatial pattern of the parameter grids. The model is first calibrated against observed streamflow at USGS gauge using CREST's built-in automatic DREAM calibration module. The objective function is set to minimize the logarithmic Nash-Sutcliffe coefficient (Table 1) for better capturing low-moderate flow values. It should be noted that log-NSE can only be used for positive flow values thus fits better for evaluation in a perennial reach, which is the case in this study. The calibration is done by varying all CREST parameters (Table A1 in Appendix) over the period from 06/01/2015 to 12/31/2018. The observed flow over the remaining period from 01/01/2019 to 10/13/2020 is used for validation. The aim of the first calibration is to assure overall water balance and flow routing in UBRB is captured by the model. To further capture the wet/dry dynamics at the nine headwater sites, the following second calibration finetunes two already calibrated routing parameters UNDER and ALPHA0 (Table A1) within a tight range of multiplier (0.8 to 1.2) over the period from 11/09/2019 to 10/13/2020. UNDER and ALPHA0 are chosen for calibration because they respectively determine the surface and sub-surface flow velocities in the overland cells. Thus, the routing in larger downstream channels is insensitive to the variation of UNDER and ALPHA0 within the tight range. The objective function herein is set to maximize the widely-used F1 score (Table 1), which is essentially a multi-objective function combining the precision and recall metrics (Table 1, Powers, 2020). Note that the F1 score is not a built-in objective function in CREST, thus this second calibration is achieved by externally coupling CREST and the SCEUA calibration algorithm (Duan et al., 1992). We also design a three-fold cross validation to examine the model performance at different potential catchments. The split of loggers for calibration and validation considers even proportions of wet and dry values in each fold. After assuring similar performances from the three scenarios, we select the calibrated parameters from the scenario with the best evaluation metrics for the final simulation.

With the calibrated parameters, the model is warmed up from 06/01/2015 to 12/31/2015 using observed forcing data. Simulation then starts on 01/01/2016 and finishes on 10/13/2020. Table 1 summarizes the statistics used to calibrate, validate, and evaluate the hydrologic performance at the USGS gauge location and in-situ logger sites.

2.5. Investigation of stream dynamics

In previous field survey studies, statistical analyses were often conduced on attributes of the active flowing networks, like stream length, discharge, number of flow origins, and connectivity (e.g., Datry et al., 2016; Godsey and Kirchner, 2014; Jensen et al., 2017). Botter and Durighetto (2020) recently developed a more versatile tool for characterizing flowing stream network. As of this study, the primary objective

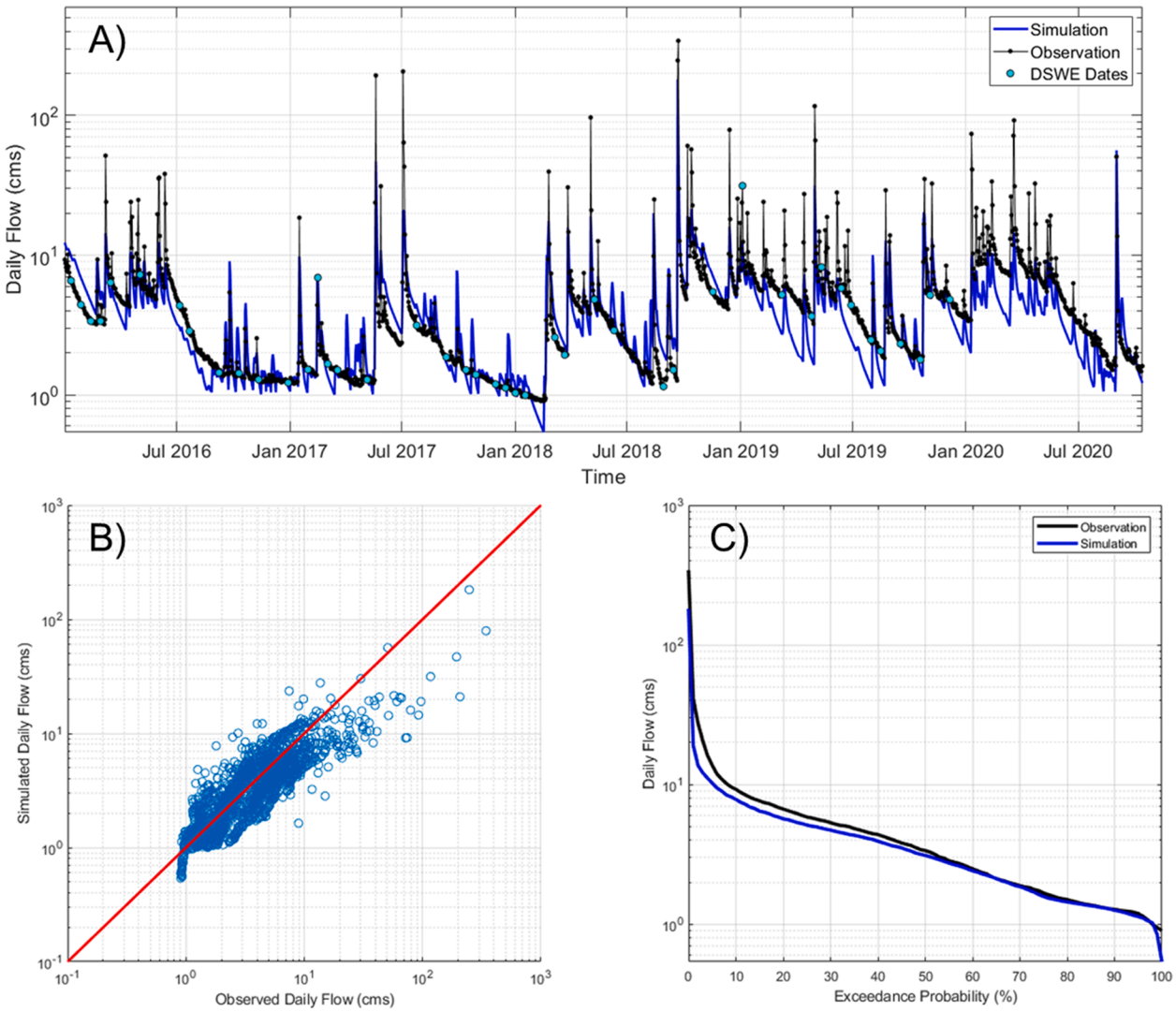

Fig. 3. Comparison of simulated and observed streamflow values at the USGS gauge location via A) time series plot in log-scale (cyan markers show dates of the used DSWE data) , B) scatter plot in log–log scale, and C) flow-duration curve in log-scale. (For interpretation of the references to color in this figure legend, the reader is referred to the web version of this article.)

Table 2
Summary of the statistical evaluations of model calibration, validation, rising limb, and falling limb of the observed hydrograph.

Hydrograph	Count	CC	RB (%)	Log-NSE
Calibration	1095	0.79	−18.9	0.87
Validation	652	0.69	−27.7	0.73
Rising Limb	464	0.79	−46.4	0.74
Falling Limb	1212	0.74	−11.6	0.85

in mapping dynamic streams is to seek hydrologic interpretation based on CREST simulation. Therefore, we select simple metrics of spatio-temporal variability of the stream water in first-level statistical analysis. First, based on the daily wet dry maps of all 10-meter pixels in the simulation domain, the average presence of water in the streams is quantified by a single metric called water occurrence (*WO*) via Eq. (1):

$$WO = \frac{\sum WD}{\sum SD} \tag{1}$$

where *WD* is water detections representing occasions (days here) with water present and SD represents simulated days. For each pixel in CREST model domain, the *WDs* are simply regarded as days with positive streamflow values.

Second, drainage density is used to measure the spatial extent of actively flowing streams across catchments of various sizes, which is defined as the total length of flowing streams per unit area of the catchment. To investigate the relationship between flowing stream length and streamflow, we examine drainage density in relation with unit discharge which is the streamflow at the most downstream stream segment of a catchment divided by the catchment area.

3. Results and discussion

3.1. Hydrologic simulation

Fig. 3A shows the simulated and observed hydrographs in log scale. Based on hydrograph shape, the low simulated and observed streamflow values show good match, while the high values are underestimated. Fig. 3B and C show the comparison via scatter plot and flow duration curves of simulated and observed streamflow, respectively. Similarly, flow values below 10 m^3/s are well captured, as indicated by scatters aligning well with the lower part of the diagonal and close match of flow duration curves near the tails. The log-NSE value of 0.79 (maximized objective function) in Table 2 indicates a satisfactory calibration

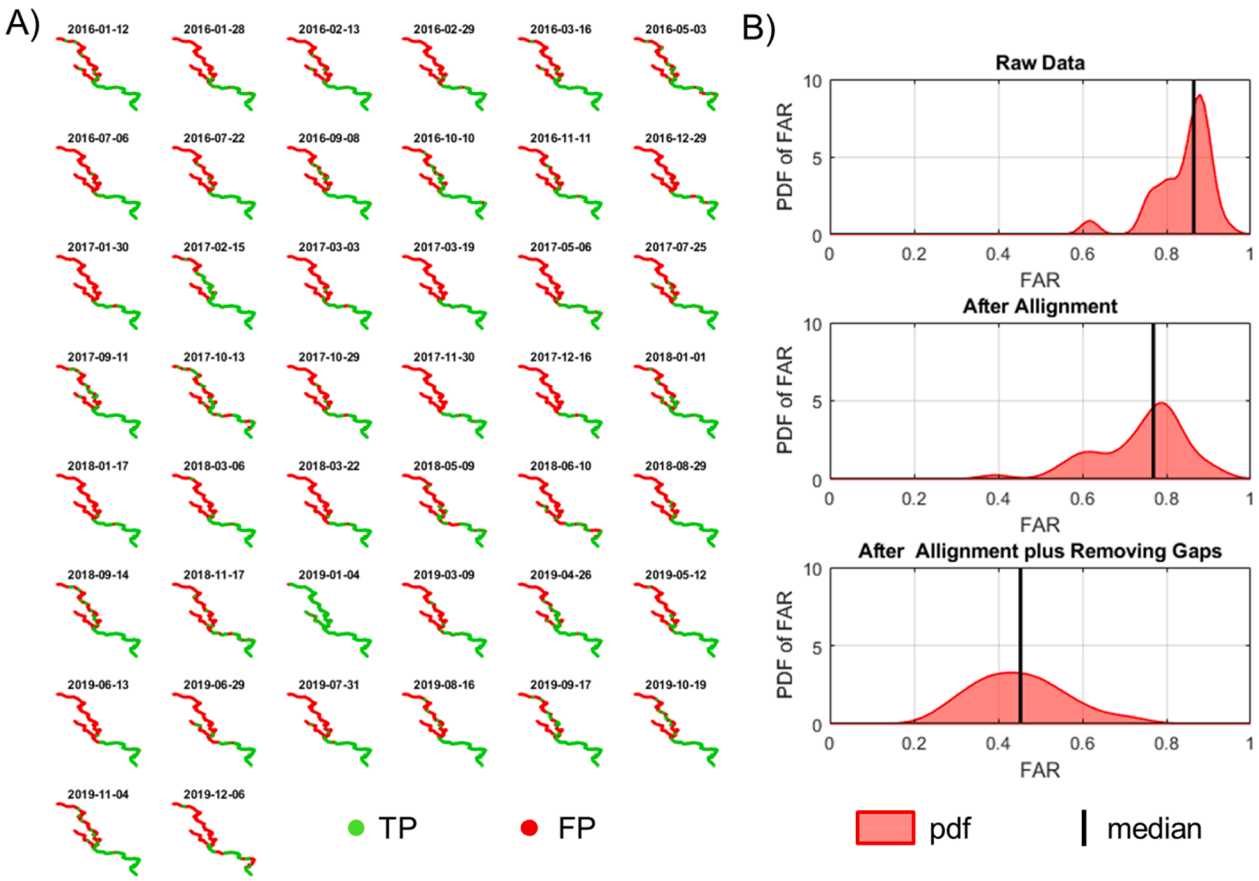

Fig. 4. A) True positives (TP) and false positives (FP) between the comparison of CREST and DSWE in streams with contributing area over 100 km^2 on the 44 cloud free days, B) probability density functions of false alarm rate (FAR) of the CREST compared with raw DSWE and DSWE after two preprocessing steps, alignment with stream cells and gap removal.

Table 3
Summary of three-fold cross validation using in-situ logger data.

Folds	Loggers for calibration	Loggers for validation	Scores		
			Precision	Recall	F1
1	1, 2, 3, 4, 7, 8	5, 6, 9	0.991	0.986	0.988
2	3, 4, 5, 6, 8, 9	1, 2, 7	0.986	0.97	0.978
3	1, 2, 5, 6, 7, 9	3, 4, 8	0.992	0.985	0.989

performance. Considering various metrics, the model performance in the calibration period is slightly better than in the validation period. The underestimation of high values also causes the overall bias to be negative. As indicated by the log-NSE values (Table 2), the model performance is better on falling limb than on the rising limb of the hydrograph. This consistently reflects the better performance on low flow values, as receding limbs span more time than rising limbs and include more low flow values.

3.2. Comparison with DSWE

Fig. 4A shows the binary comparisons between CREST simulation and preprocessed DSWE in streams with contributing area great than 100 km^2. The comparison only results in two cases, TP, and FP, as these streams are simulated to be perennial by the CREST model. It can be found that the detection of water by DSWE in the main stem (contributing area $>$ 300 km^2) is unstable with discontinuous segments; and water-covered pixels in the two upstream tributaries are even more sporadic. This is due to the narrow stream width, which reduces to around 5 m just upstream of the confluence and possibly reaches the limit of DSWE's detectability. The only exceptions occurred on 02/15/2017 and 01/04/2019, corresponding to high flow values observed at the downstream USGS gauge (Fig. 3A). The high flow causes streams to become wider and detectable by the DSWE. Fig. 4B shows that preprocessing reduces the false positive rate to around 0.5 by essentially filling the discontinuous patches (removing FP cases) in the main stem. In summary, DSWE fails to detect flowing streams narrower than 10 m and inconsistently detect water presence in channels around 15-meter wide.

3.3. Validation using In-Situ loggers

The results of validating metrics for the threefold cross validation using in-situ loggers are presented in Table 3. All three scenarios result in very high precision, recall, and F1 values. The three folds show equally high scores, indicating the three separately calibrated models can perform comparably on the testing datasets. This illustrates the model's ability to perform well with an unseen dataset in potentially a different headwater catchment.

3.4. Stream dynamics mapping

Fig. 5A shows the monthly time series of areal-averaged precipitation and PET of UBRB over the 4-year period. There is a noticeable interannual change in precipitation across the four years with year 2018 being the wettest. Seasonal variation is also evident where spring (March, April, and May) has the most precipitation followed by either summer (June, July, and August) or fall (September, October, and November) and then winter (December, January, and February). Also, summer months feature hot and dry days with high PET values (Fig. 5B).

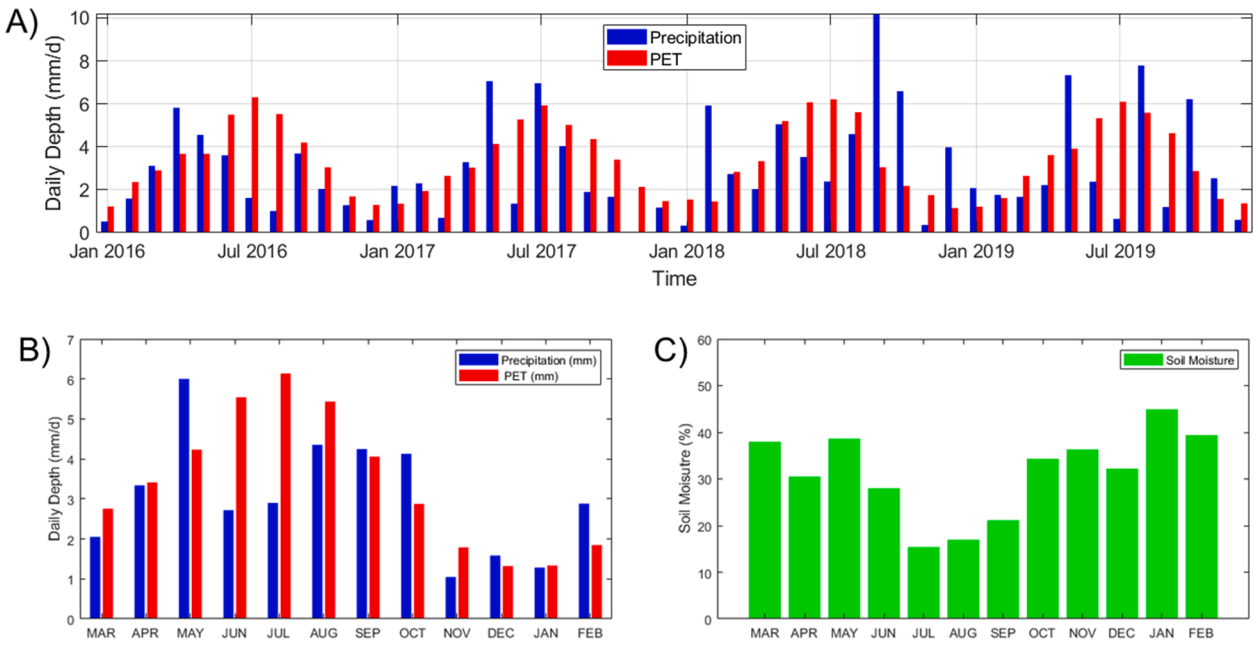

Fig. 5. A) Monthly time series of mean-basin precipitation and PET of UBRB in 2016 to 2019, temporally averaged mean-basin B) precipitation and PET and C) soil moisture for the 12 months. Precipitation and PET are input forcing data, while soil moisture is a model state and an output from the CREST simulation.

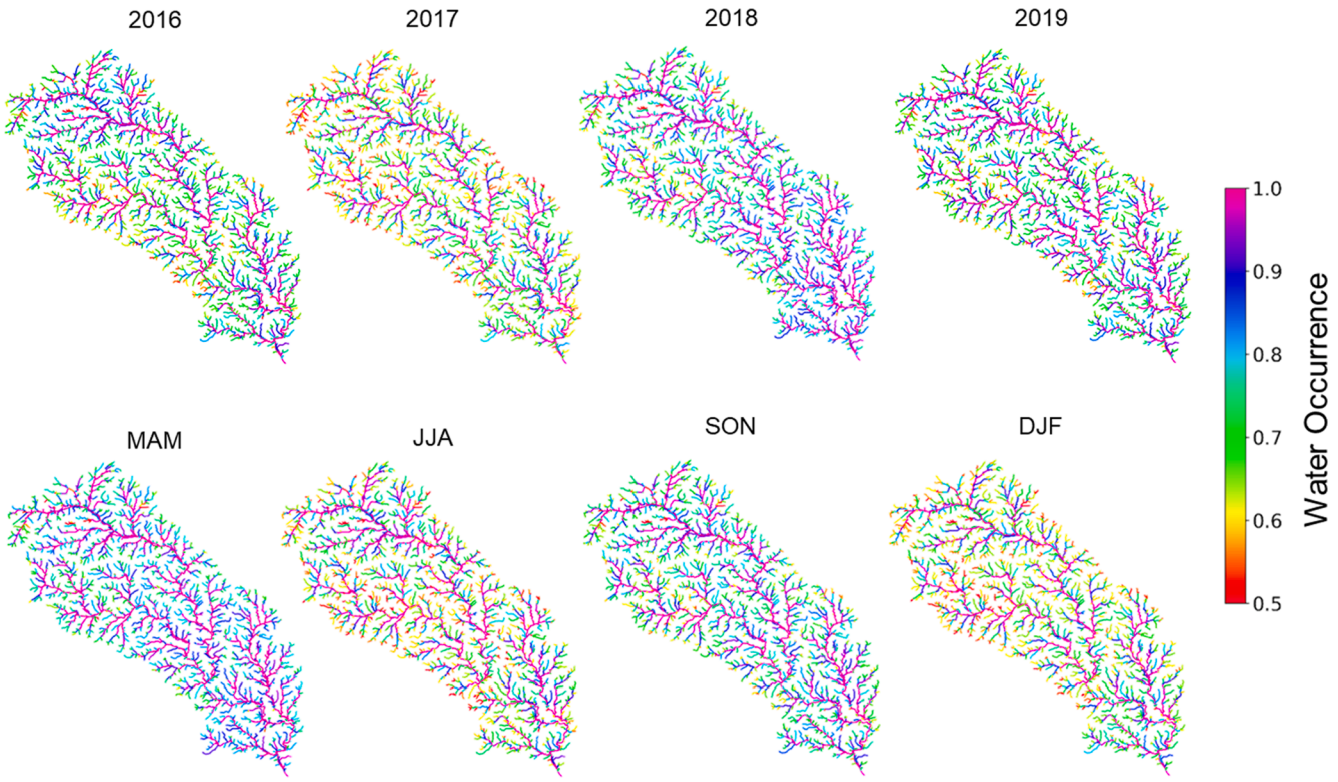

Fig. 6. Water occurrence calculated based on CREST simulation in 2510 stream segments for the four years and four seasons.

As a result of both precipitation and PET, the soil moisture shows clear seasonal pattern with highest soil moisture occurring in winter followed by spring and fall; soils are dry in summer with a soil moisture value nearly half of that in winter (Figs. 5C and 7).

Using four years of daily streamflow grids output, we map the water occurrence over the 2510 stream segments in UBRB for the four years and the four seasons (Fig. 6). Table 4 summarizes mean annual and seasonal water occurrence conditioned on contributing area for small headwater catchments. Streams with contributing area over ~5 km^2 appear to have flow over 77% of the time during the four years. Smallest tributaries in the headwater catchments (contributing area < 0.2 km^2) are mostly non-perennial with active flow for 78% percent of the time. In terms of stream length, 18% the total 1145 km of stream length stays perennial during the four years. Across the seasons, streams show the highest water occurrence in the spring followed by fall, summer, and winter. This can be explained by the seasonal variability of precipitation

Table 4
Summary of stream intermittency metrics of headwater tributaries conditioned on drainage area.

Water Occurrence		Contributing Area (km^2)				
		<0.2	0.2 ~ 0.5	0.5 ~ 1	1 ~ 2	2 ~ 5
Years	2016	0.78	0.80	0.79	0.82	0.82
	2017	0.73	0.75	0.74	0.77	0.77
	2018	0.81	0.83	0.82	0.85	0.85
	2019	0.79	0.80	0.79	0.83	0.83
Seasons	Spring	0.72	0.79	0.87	0.93	0.94
	Summer	0.57	0.66	0.78	0.87	0.90
	Fall	0.65	0.73	0.83	0.90	0.92
	Winter	0.57	0.64	0.74	0.83	0.88

and PET as shown in Fig. 5A. In terms of precipitation, the wettest season is spring (3.8 mm/d), followed by summer (3.33 mm/d), fall (3.15 mm/d), and winter (1.88 mm/d). Summer features high PET (5.7 mm/d), offsetting the intense but infrequent precipitation (Li et al., 2012), and resulting in overall lower runoff, as compared to fall with an averaged PET of only 2.9 mm/d. This effect is also evident in storage dynamics of the watershed as shown by the monthly time series of soil moisture in Fig. 5C. The high PET reduces antecedent soil moisture ahead of storm events and further decreases the overland runoff generation. In contrast, low PET in winter makes the soil moisture higher than in any other season (Fig. 5C and Fig. 7) despite the lowest precipitation. This causes the water occurrence of streams in winter season to be only slightly smaller than that in the summer season.

Fig. 7 shows the seasonally averaged soil moisture simulated by CREST, where two areas (outlined) with different hydrologic responses are selected to illustrate the heterogeneous effects of geographical properties on stream dynamics. Fig. 8A and 8B show the monthly mean areal water occurrence and soil moisture for the two areas, respectively. In all seasons but summer, soil moisture in Area B is higher than in Area A. In Area B, the dramatic drop of soil moisture in summer also coincides with the sudden decrease of water occurrence, as seen in August 2016, July 2018 and July 2019. Such discrepancy in the hydrologic response is due to the different soil and land types of the two areas, as shown in Fig. 1. Area A features a more impervious surface plus sandy soils which hold low soil water content, whereas Area B is a naturalized catchment with clayey soils of high water-holding capacity. In summer, limited evapotranspiration occurs in the Area A due to its impervious coverage. The soil moisture in Area A is thus less sensitive than in Area B (Fig. 8B). Fig. 8C and D show the monthly composition of surface and subsurface runoff in Area A and B, respectively. The dotted lines mark the 50% value, and no color signifies months without rainfall input. It can be found that the different land cover and soil properties cause Area A and Area B to be dominated by surface and subsurface runoff, respectively. The higher proportion of surface runoff in Area A could also be the

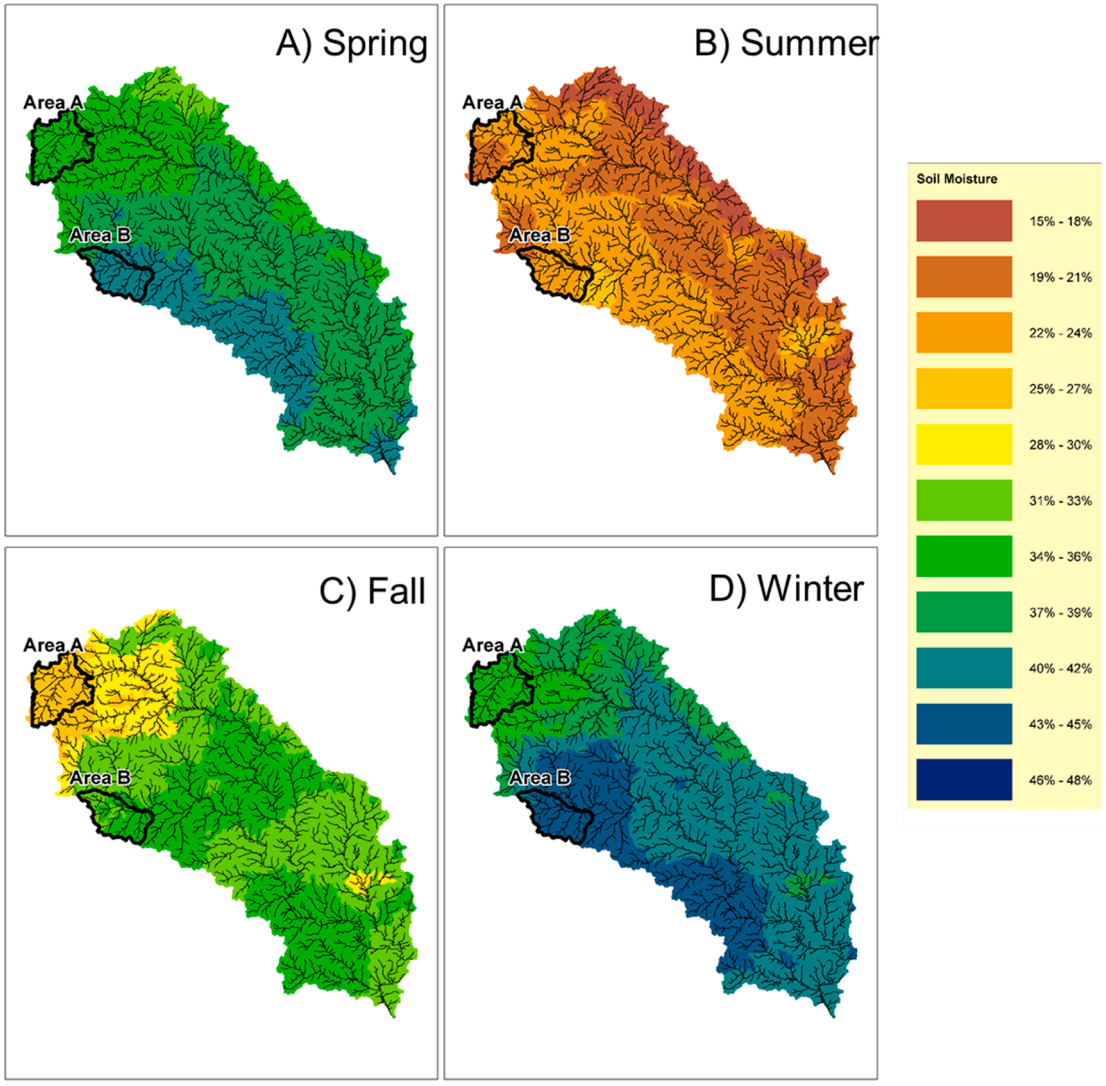

Fig. 7. Time-averaged soil moisture calculated based on CREST simulation in Spring (A), Summer (B), Fall (C) and Winter (D) from 2016 to 2019.

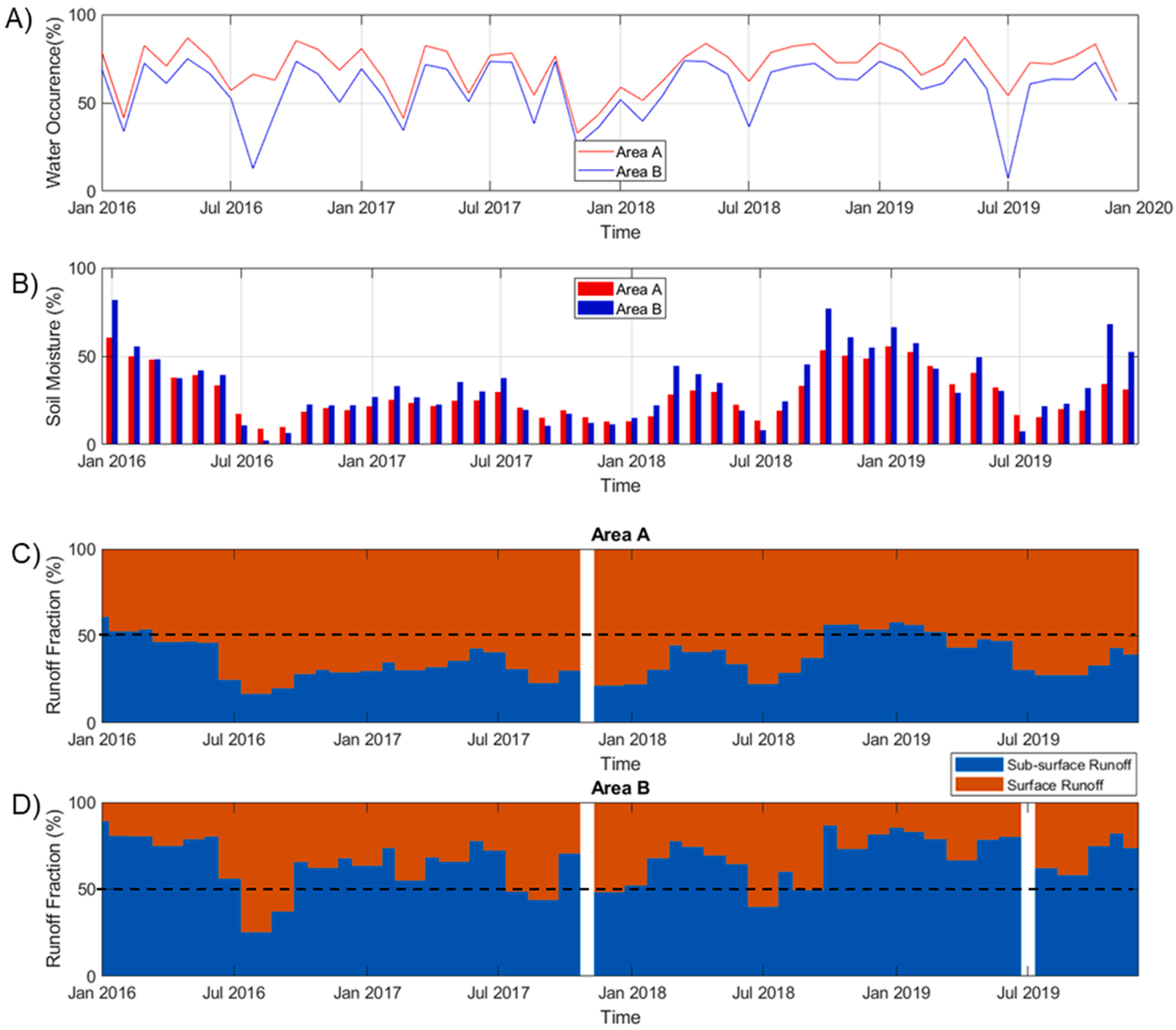

Fig. 8. Monthly time series of space–time-averaged (A) water occurrence, (B) soil moisture, and (C and D) fractional surface and subsurface runoff in Area A and B.

reason for the overall higher water occurrence. Although subsurface runoff dominates in Area B, a few switches in the runoff generation mechanism can be found in summer when surface runoff composition gets above 50%. Such switches coincide with lowest soil moisture values, since whatever small amount of infiltration is stored as soil water instead of running off. In terms of land cover and soil types, Area B is representative of the whole UBRB (Fig. 1), suggesting a large fraction of the watershed is as sensitive as Area B and likely to experience similar seasonal switches in runoff generation mechanism.

We also examine the relationships between streamflow and drainage density in 16 selected catchments, as shown in Fig. 9. The selection incorporates three levels of catchments sizes (10 to 20, 50 to 60, and near 120 km^2) and assures that catchments are independent within each level and spread evenly over the UBRB. Across the three levels, drainage density, as plotted in Fig. 9A to C, increases roughly as power functions of unit discharge below some threshold values (about 10^{-2} mm/d) and plateaus beyond the threshold. In log–log scale, the values below the threshold are also fitted to linear relationships for each individual catchment. The fitted relationships show strong statistical significance as indicated by the high R^2 (coefficient of determination) values (Table 5). For basins of various sizes, the log–log slope k values (exponent in the power-law relationships) are similar (0.31 to 0.4) while the log–log intercepts (b) range from 0.91 to 1.23. Variability in drainage density at a given unit discharge (the spread along the vertical direction) reduces with increasing catchment size as tributaries merge at confluences and form larger streams.

3.5. Discussion

Both streamflow in high-order streams and wet/dry status in headwater tributaries are automatically calibrated in this study. Automatic calibration scheme allows multi-objective cost functions and is appropriate/necessary for intermittent catchments (Azarnivand et al., 2020b), like the F1 score used for calibration using in-situ logger data. The underestimation of high flow values by the CREST model is mainly due to the daily simulation time step (Fohrer et al., 2001). During high flow events (flooding), the timing and magnitude of flood peaks are sensitive to the temporal distribution of rainfall. Because of the non-linearities in the water balance and routing processes, the daily average rainfall intensity diffuses any sub-daily variabilities and is too coarse for simulating streamflow during floods. Also, in overland routing scheme (kinematic wave), travel time from one grid cell to next downstream

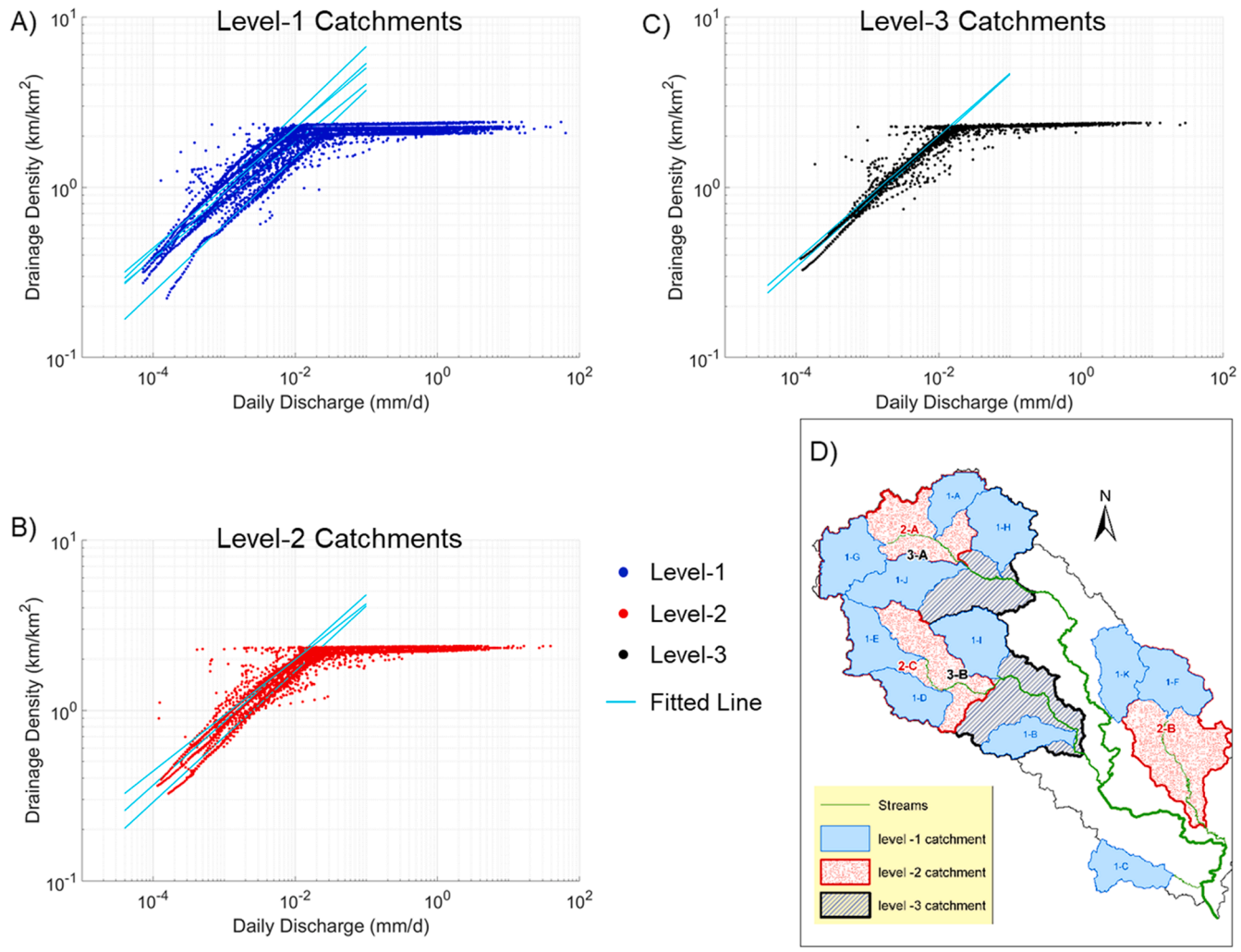

Fig. 9. Scaling relationships between drainage density and unit discharge in (A) level-1, (B) level-2, and (C) level-3 catchment; (D) map of the catchments on three levels.

Table 5
Summary of the catchments in which scaling relationship between drainage density and unit discharge is examined; k is the scaling exponent; b is the intercept in log-scale; and R^2 is the coefficient of determination.

Level	Name	Contributing Area (km^2)	k	b	R^2
1	1-A	11.6	0.32	0.94	0.85
	1-B	11.7	0.32	0.95	0.96
	1-C	13.2	0.36	1.10	0.96
	1-D	14.4	0.40	1.20	0.87
	1-E	16.6	0.34	1.02	0.90
	1-F	17.6	0.35	1.05	0.94
	1-G	19.3	0.40	0.97	0.90
	1-H	19.1	0.40	1.23	0.92
	1-I	20.5	0.38	1.11	0.91
	1-J	23.6	0.34	0.95	0.87
	1-K	24.6	0.37	0.91	0.90
2	2-A	56.4	0.38	1.00	0.91
	2-B	55.6	0.33	0.95	0.88
	2-C	58	0.37	1.05	0.80
3	3-A	119.3	0.38	1.04	0.91
	3-B	119.9	0.37	1.03	0.85

shortens with increasing unit discharge. During floods, the daily time step is at a larger scale than the travel time between 10-meter grid cells. Such effect also propagates downstream, causing the translated volume to reduce at higher order streams. The underestimation of high flow has not been widely reported by other modeling studies that investigate intermittent catchments using also daily timestep, probably due to the relatively small catchment size and short channel length (e.g., Niedda and Pirastru, 2014; Pierini et al., 2014; Camporese et al., 2014; Dean et al., 2016). In comparison with distributed models, lumped models could deal with this issue with flexibility, for instance, by using duration-specific unit hydrographs. However, the trade-off is the inability to simulate streamflow at any point within the catchment like the distributed models.

The interannual and seasonal variabilities of the rainfall and PET are well reflected in stream dynamics in UBRB (Fig. 6). The role of rainfall intensity and frequency have been demonstrated to be vital for stream dynamics in intermittent catchments by previous studies (Azarnivand et al., 2020a, Dean et al., 2016). The contrast of water occurrence in summer and fall indicates mutual effects of rainfall, PET, and soil

moisture on runoff generation. Interestingly, the seasonality in forcings is strong enough to switch runoff generation mechanism in headwater tributaries across wet and dry periods (Fig. 8D), which is also revealed by previous studies on the blue river basin (Li et al., 2012; Tian et al., 2012). The heterogeneity in catchment characteristics cause distinction in water occurrence of head tributaries (Fig. 8), via the distribution of surface and subsurface runoff. This strengthens the significance of antecedent catchment wetness prior to rainfall events in driving streamflow in intermittent catchments, as also reported in previous studies (Viola et al., 2014; Niedda and Pirastru, 2014).

Although not fully exposed in the UBRB, the CREST model lacks representation of certain physical processes at fine spatial resolution (e.g. 10 m), which might become issues in other study areas. For instance, in low-yielding basins in the western U.S., additional abstraction storage needs to be included to represent ground surface depression and soil shrinkage cracks. In terms of groundwater, the CREST model adopts a conceptual bucket module to represent the recharge and discharge of groundwater, in which groundwater flow is assumed to be parallel to the surface topography. The bucket concept is also widely used in other distributed hydrologic and land surface models (Niu et al., 2011) as a simplification of the highly heterogeneous and nonlinear groundwater flow process, because an explicit representation of these processes is currently limited by the lack of information on bedrock topography (Camporese et al., 2019) and the difficulty to assign spatially and vertically distributed parameters (Maneta et al., 2008). Also, this assumption exempts the assignment of boundary conditions because groundwater is assumed to move only within the watershed boundary free from influence of surrounding hydraulic heads. However, there would be issues when the extent of underlying aquifer significantly exceeds the watershed boundary or when surface flow originates in aquifer-fed springs.

The scaling relationships between drainage density and unit discharge have been reported in studies based on field mapping (Godsey and Kirchner, 2014; Gregory and Walling, 1968). Due to the low frequency of mapping and logistical challenges, the mapped stream networks are subject to issues like low statistical significance, limited spatial coverage of mapped networks in complex terrain, and influences from stochastic factors (e.g., debris and sediment collected by tree falls). As demonstrated in this study, hydrologic modeling here confirms and augments the power-law relationship of strong statistical significance by continuously generating data at high resolution over a large spatial scale. The scaling relationships plateau at some threshold discharge values, representing entirely active stream networks at high flow conditions. The existence of some plateau is reasonable because it physically represents the geomorphic channel networks, i.e., the branching networks of topographic features. Nonetheless, the plateaus, which correspond to the size (total length) of stream networks, are limited by the resolution of topographic data (DEM). In other words, the total length of streams could have exponentially increased and allowed the power-law relationship to extend further, had the model been simulated over finer grids, e.g., using 1-meter DEM. To certain extent, the plateau also justifies the underestimation of high flow by the CREST model, as stream dynamics is demonstrated to be only sensitive to discharge at low-moderate flow conditions.

4. Conclusions

In this study, we demonstrate the capability of distributed hydrologic modeling to capture the stream dynamics in upper Blue River basin, OK. The fully-distributed CREST model is established over 10-meter grids using distributed geographic data, forcing data, and parameters of fine resolution. The high spatial resolution of the simulation enables us to decipher dynamics in refined stream networks with the averaged contributing area of individual stream segment being <0.2 km^2. The large spatial scale of study area exceeds most of existing studies and allows us to examine the stream dynamics across a wide range of stream orders and catchment sizes and potentially capture effects from heterogenous catchment characteristics. To achieve desired model performance at various stream orders, we deploy in-situ state loggers at nine headwater tributaries as an additional calibration/validation source to the USGS stream gauge. We also explore the utility of LANDSAT product DSWE in capturing water presence in high-order channels. Output streamflow grids are lastly used to map actively flowing stream networks at daily time step. The mapped stream networks are interpreted hydrologically using the gridded output from the CREST model. The major findings are summarized as follows.

1. The hydrologic simulation at 10-meter spatial resolution and daily temporal resolution using the CREST model performs well against low/moderate observed flow, as indicated by a logarithmic NSE over 0.7 in the validation period. Due to the daily timestep, high flow values are underestimated. At headwater tributaries, the calibrated simulation can accurately capture wet/dry status, as compared with in-situ logger records.
2. The 30-meter LANDSAT Dynamic Surface Water Estimate (DSWE) products are insufficient to serve as validation source for water presence even in high order streams after preprocessing is applied. Due to limitation in resolution, the data only detect discontinuous patches of water in 15-meter-wide streams and sporadic water presence in 10-meter-wide streams.
3. Flowing stream networks are dynamic over the 4-year simulation period in UBRB. At daily time step, the density of flowing stream length scales as a power-law function of unit discharge below a threshold value. Above the threshold, the whole networks become active with flowing water. The existence of the threshold also justifies the underestimation of high flow values by the CREST, as stream dynamics is sensitive only to low-moderate unit discharges. The exponent of the power-law relationship i.e., change in drainage density per change in unit discharge, stays consistent across catchments of various sizes, indicating the existence of a central tendency across the numerous streams in UTRB.
4. Mapping of water occurrence shows that streams are most dynamic in the small headwater catchments. The interannual and seasonal variabilities of precipitation and PET is well reflected by the water occurrence in these small non-perennial tributaries. The distinction in land cover and soil properties cause the runoff generation mechanism to differ among heterogenous headwater catchments, which indicates the significance of antecedent catchment wetness prior to rainfall events in driving streamflow in non-perennial catchments.

Compared with traditional field mapping approach in stream dynamics study, the modeling approach can generate data samples with greater statistical significance, temporal frequency, and range. Therefore, distributed hydrologic models should be utilized more to understand controls on the sensitivity of the flowing stream networks to changes in runoff. This study also reveals the need for future research efforts, since hydrological modeling of intermittent streams is very much constrained by the quantity and quality of observations needed to calibrate and validate the model outputs. Therefore, as a-priori estimates from this study, the simulated output needs to be supplemented with better datasets. Also models in general are only as good as our understanding of the physical processes that drive stream dynamics. The representation of physical processes is also sensitive to model resolution. At fine scales, additional processes need to be included and represent complex nonlinear processes of runoff generation in low-yielding basins, e.g. surface–groundwater interactions or local geological peculiarities like karstic areas (Ye et al., 1997). Following this study, ongoing research focuses on coupling CREST with land surface models to represent springs fed by unconfined aquifers in arid and karstic basins. Finally, as we are confident that the mapped dynamic stream networks make sense hydrologically, a more in-depth future study focusing on stream dynamics will follow to take advantage of the rich information in

the CREST simulation using more complex statistical tools.

CRediT authorship contribution statement

Shang Gao: Conceptualization, Data curation, Formal analysis, Methodology, Investigation, Software, Validation, Writing - original draft, Writing - review & editing. **Mengye Chen:** Methodology, Investigation, Writing - review & editing. **Zhi Li:** Methodology, Investigation, Writing - review & editing. **Stephen Cook:** Methodology, Investigation, Data curation, Writing - review & editing. **Daniel Allen:** Conceptualization, Writing - review & editing. **Thomas Neeson:** Conceptualization, Writing - review & editing. **Titantian Yang:** Methodology, Writing - review & editing. **Teshome Yami:** Supervision, Writing - review & editing. **Yang Hong:** Conceptualization, Methodology, Supervision, Writing - review & editing.

Declaration of Competing Interest

The authors declare that they have no known competing financial interests or personal relationships that could have appeared to influence the work reported in this paper.

Acknowledgment

The authors would like to thank four anonymous reviewers for their constructive and insightful comments that helped to improve this study. The authors would also like to thank the funding support from National Science Foundation (Project number: 1802872) and the funding support from the National Science Foundation (Project No. OIA-1946093 and its subaward No. EPSCoR-2020-3).

Appendix

Preprocessing of DSWE

Preprocessing is conducted on DSWE prior to the validation following the steps below. First, Digital Elevation Model (DEM) data in CREST, like most of distributed hydrologic models, are filled to avoid water from being trapped locally. Ponds and potholes should thus be excluded from validation. We automatically segment ponds from the DSWE rasters using an algorithm traditionally applied in identifying rain cells from radar images (Dixon and Wiener, 1993) and then filtering the identified clusters of water-covered pixels considering their shape and area. After fitting identified pixel clusters to ellipsoids, we exclude those with ellipticity (ratio of minor axis over major axis) lower than 0.2 and area above 9,000 m^2. Next, we align the stream cells in DSWE rasters with those in the CREST domain by nudging adjacent inundated DSWE pixels into CREST streams while limiting the nudging distance to be 30 m (one DSWE pixel). This step is crucial because the CREST streamflow output is 1-D, which means one stream cell and its adjacent overland cells could have significantly different contributing area and stream flow. Therefore, a DSWE water-covered pixel is paired (aligned) with a nearby stream cell for the comparison. Lastly, the water-covered pixels in DSWE can be discontinuous even after the alignment (Fig. A1), which can be interpreted as isolated pools in small streams but are unlikely to occur in high-order streams with persistent baseflow. Another cause for the discontinuity is no-data stripes of unscanned pixels that cut through stream networks and leave many no-data gaps. In order to quantify the effect from the discontinuous features in higher-order streams, we fill the gaps between two adjacent water-covered segments that are separated by <90 m of flow distance (distance along streams) and have drainage area over 300 km^2. With the preprocessing done, DSWE rasters are resampled using nearest neighbor approach to 10-meter resolution and then compared with CREST streamflow grids.

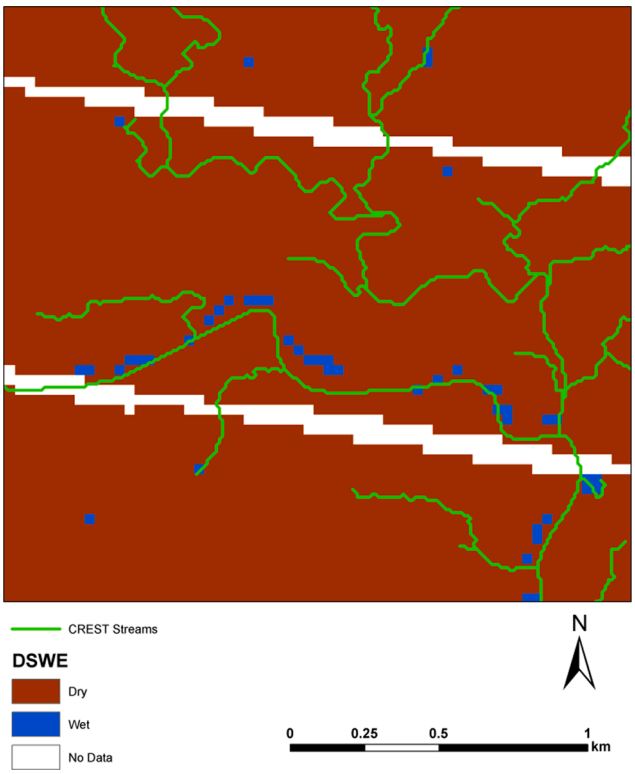

Fig. A1. Example of DSWE dataset with challenging issues for validating hydrologic modeling.

Table A1

Parameter	Category	Min	Max	Brief Description
WM	WaterBalance	5	250	Maximum soil water capacity (depth integrated pore space) of the model soil layer in millimeters
B		0.1	20	Exponent of the variable infiltration curve
IM		0.01	5	Impervious area ratio
KE		0.001	1	Adjustment factor to PET grids
FC		0	150	Soil saturated hydraulic conductivity in mm/hr
TH	Routing	30 km^2	300 km^2	Threshold for how many cells must drain into a cell for it to be considered part of a river
UNDER		0.0001	3	Interflow flow speed multiplier
LEAKI		0.01	1	Amount of water leaking out of the interflow reservoir at each time step
ALPHA		0.001	3	Multiplier in the kinematic equation $Q = \alpha A^{\beta}$ for channel cells
BETA		0.001	1	Exponent in the kinematic equation $Q = \alpha A^{\beta}$ for channel cells
ALPHA0		0.001	5	Multiplier in the kinematic equation $Q = \alpha A^{\beta}$ for overland cells

References

Allen, D.C., et al., 2020. River ecosystem conceptual models and non-perennial rivers: A critical review. Wiley Interdisciplinary Reviews: Water 7 (5), e1473.
Azarnivand, A., Camporese, M., Alaghmand, S., Daly, E., 2020a. Modeling hydrological impacts of afforestation on intermittent streams. Sci. Total Environ. 728, 138748.
Azarnivand, A., Camporese, M., Alaghmand, S., Daly, E., 2020b. Simulated response of an intermittent stream to rainfall frequency patterns. Hydrol. Process. 34 (3), 615–632.

Benstead, J.P., Leigh, D.S., 2012. An expanded role for river networks. Nat. Geosci. 5 (10), 678–679.
Bhamjee, R., Lindsay, J., 2011. Ephemeral stream sensor design using state loggers. Copernicus. Publications.
Bishop, K., et al., 2008. Aqua Incognita: the unknown headwaters. Hydrol. Process. 22 (8), 1239.
Botter, G., Durighetto, N., 2020. The Stream Length Duration Curve: a tool for characterizing the time variability of the flowing stream length. Water resources research, 56(8): e2020WR027282.
Brown, S.C., Versace, V.L., Lester, R.E., Walter, M.T., 2015. Assessing the impact of drought and forestry on streamflows in south-eastern Australia using a physically based hydrological model. Environmental Earth Sciences 74 (7), 6047–6063.
Busch, M.H., et al., 2020. What's in a Name? Patterns, Trends, and Suggestions for Defining Non-Perennial Rivers and Streams. Water 12 (7), 1980.
Camporese, M., Daly, E., Dresel, P.E., Webb, J.A., 2014. Simplified modeling of catchment-scale evapotranspiration via boundary condition switching. Adv. Water Resour. 69, 95–105.
Camporese, M., Paniconi, C., Putti, M., McDonnell, J.J., 2019. Fill and spill hillslope runoff representation with a Richards equation-based model. Water Resour. Res. 55 (11), 8445–8462.
Chahinian, N., Tournoud, M.-G., Perrin, J.-L., Picot, B., 2011. Flow and nutrient transport in intermittent rivers: a modelling case-study on the Vène River using SWAT 2005. Hydrological Sciences Journal-Journal des Sciences Hydrologiques 56 (2), 268–287.
Chapin, T.P., Todd, A.S., Zeigler, M.P., 2014. Robust, low-cost data loggers for stream temperature, flow intermittency, and relative conductivity monitoring. Water Resour. Res. 50 (8), 6542–6548.
Cipriani, T., Tilmant, F., Branger, F., Sauquet, E., Datry, T., 2014. Impact of climate change on aquatic ecosystems along the Asse river network. FRIEND-Water 2014, Hydrology in a Changing World: Environmental and Human Dimensions: 463-468.
Constantz, J., Stonestorm, D., Stewart, A.E., Niswonger, R., Smith, T.R., 2001. Analysis of streambed temperatures in ephemeral channels to determine streamflow frequency and duration. Water Resour. Res. 37 (2), 317–328.
Costa, A.C., Foerster, S., de Araújo, J.C., Bronstert, A., 2013. Analysis of channel transmission losses in a dryland river reach in north-eastern Brazil using streamflow series, groundwater level series and multi-temporal satellite data. Hydrol. Process. 27 (7), 1046–1060.
Costelloe, J.F., Grayson, R.B., McMahon, T.A., 2005. Modelling stream flow for use in ecological studies in a large, arid zone river, central Australia. Hydrological Processes: An International Journal 19 (6), 1165–1183.
Costigan, K.H., et al., 2017. Flow regimes in intermittent rivers and ephemeral streams. Intermittent rivers and ephemeral streams. Elsevier 51–78.
Daneshmand, H., Alaghmand, S., Camporese, M., Talei, A., Daly, E., 2019. Water and salt balance modelling of intermittent catchments using a physically-based integrated model. J. Hydrol. 568, 1017–1030.
Daneshmand, H., et al., 2020. Long-term impacts of partial afforestation on water and salt dynamics of an intermittent catchment under climate change. Water 12 (4), 1067.
Datry, T., 2012. Benthic and hyporheic invertebrate assemblages along a flow intermittence gradient: effects of duration of dry events. Freshw. Biol. 57 (3), 563–574.
Datry, T., Larned, S.T., Tockner, K., 2014. Intermittent rivers: a challenge for freshwater ecology. Bioscience 64 (3), 229–235.
Datry, T., Pella, H., Leigh, C., Bonada, N., Hugueny, B., 2016. A landscape approach to advance intermittent river ecology. Freshw. Biol. 61 (8), 1200–1213.
De Girolamo, A., Lo Porto, A., Pappagallo, G., Tzoraki, O., Gallart, F., 2015. The hydrological status concept: application at a temporary river (Candelaro, Italy). River Res. Appl. 31 (7), 892–903.
Dean, J., et al., 2016. Water balance complexities in ephemeral catchments with different land uses: Insights from monitoring and distributed hydrologic modeling. Water Resour. Res. 52 (6), 4713–4729.
Dixon, M., Wiener, G., 1993. TITAN: Thunderstorm identification, tracking, analysis, and nowcasting—A radar-based methodology. J. Atmos. Oceanic Technol. 10 (6), 785–797.
Duan, Q., Sorooshian, S., Gupta, V., 1992. Effective and efficient global optimization for conceptual rainfall-runoff models. Water Resour. Res. 28 (4), 1015–1031.
Durighetto, N., Vingiani, F., Bertassello, L.E., Camporese, M., Botter, G., 2020. Intraseasonal drainage network dynamics in a headwater catchment of the Italian Alps. Water Resources Research, 56(4): e2019WR025563.
Eng, K., Wolock, D.M., Dettinger, M., 2016. Sensitivity of intermittent streams to climate variations in the USA. River Res. Appl. 32 (5), 885–895.
Fatichi, S., et al., 2016. An overview of current applications, challenges, and future trends in distributed process-based models in hydrology. J. Hydrol. 537, 45–60.
Fohrer, N., Haverkamp, S., Eckhardt, K., Frede, H.-G., 2001. Hydrologic response to land use changes on the catchment scale. Phys. Chem. Earth Part B 26 (7–8), 577–582.
Gassman, P.W., Reyes, M.R., Green, C.H., Arnold, J.G., 2007. The soil and water assessment tool: historical development, applications, and future research directions. Trans. ASABE 50 (4), 1211–1250.
Gleason, C.J., Smith, L.C., 2014. Toward global mapping of river discharge using satellite images and at-many-stations hydraulic geometry. Proc. Natl. Acad. Sci. 111 (13), 4788–4791.
Godsey, S., Kirchner, J.W., 2014. Dynamic, discontinuous stream networks: hydrologically driven variations in active drainage density, flowing channels and stream order. Hydrol. Process. 28 (23), 5791–5803.
Goulsbra, C., Evans, M., Lindsay, J., 2014. Temporary streams in a peatland catchment: pattern, timing, and controls on stream network expansion and contraction. Earth Surf. Proc. Land. 39 (6), 790–803.
Gregory, K., Walling, D., 1968. The variation of drainage density within a catchment. Hydrol. Sci. J. 13 (2), 61–68.
Hamada, Y., O'Connor, B.L., Orr, A.B., Wuthrich, K.K., 2016. Mapping ephemeral stream networks in desert environments using very-high-spatial-resolution multispectral remote sensing. J. Arid Environ. 130, 40–48.
Ivkovic, K., Croke, B., Kelly, R., 2014. Overcoming the challenges of using a rainfall–runoff model to estimate the impacts of groundwater extraction on low flows in an ephemeral stream. Hydrol. Res. 45 (1), 58–72.
James, N.A., Matteson, D.S., 2013. ecp: An R package for nonparametric multiple change point analysis of multivariate data. arXiv preprint arXiv:1309.3295.
Jensen, C.K., McGuire, K.J., McLaughlin, D.L., Scott, D.T., 2019. Quantifying spatiotemporal variation in headwater stream length using flow intermittency sensors. Environ. Monit. Assess. 191 (4), 1–19.
Jensen, C.K., McGuire, K.J., Prince, P.S., 2017. Headwater stream length dynamics across four physiographic provinces of the A ppalachian H ighlands. Hydrol. Process. 31 (19), 3350–3363.
Jones, J.W., 2019. Improved automated detection of subpixel-scale inundation—Revised dynamic surface water extent (dswe) partial surface water tests. Remote Sensing 11 (4), 374.
Larned, S.T., Datry, T., Arscott, D.B., Tockner, K., 2010. Emerging concepts in temporary-river ecology. Freshw. Biol. 55 (4), 717–738.
Li, H., Sivapalan, M., Tian, F., 2012. Comparative diagnostic analysis of runoff generation processes in Oklahoma DMIP2 basins: The Blue River and the Illinois River. J. Hydrol. 418, 90–109.
Liang, X., Lettenmaier, D.P., Wood, E.F., Burges, S.J., 1994. A simple hydrologically based model of land surface water and energy fluxes for general circulation models. Journal of Geophysical Research: Atmospheres 99 (D7), 14415–14428.
Lovill, S., Hahm, W., Dietrich, W., 2018. Drainage from the critical zone: lithologic controls on the persistence and spatial extent of wetted channels during the summer dry season. Water Resour. Res. 54 (8), 5702–5726.
Maneta, M., Schnabel, S., Jetten, V., 2008. Continuous spatially distributed simulation of surface and subsurface hydrological processes in a small semiarid catchment. Hydrological Processes: An International Journal 22 (13), 2196–2214.
Matteson, D.S., James, N.A., 2014. A nonparametric approach for multiple change point analysis of multivariate data. J. Am. Stat. Assoc. 109 (505), 334–345.
Meerveld, H., Kirchner, J.W., Vis, M.J., Assendelft, R.S., Seibert, J., 2019. Expansion and contraction of the flowing stream network alter hillslope flowpath lengths and the shape of the travel time distribution. Hydrol. Earth Syst. Sci. 23 (11), 4825–4834.
Nash, J., 1957. The form of the instantaneous unit hydrograph. International Association of Scientific Hydrology, Publ 3, 114–121.
Niedda, M., Pirastru, M., 2014. Field investigation and modelling of coupled stream discharge and shallow water-table dynamics in a small Mediterranean catchment (Sardinia). Hydrol. Process. 28 (21), 5423–5435.
Niu, G.Y., et al., 2011. The community Noah land surface model with multiparameterization options (Noah-MP): 1. Model description and evaluation with local-scale measurements. Journal of Geophysical Research: Atmospheres 116 (D12).
Peirce, S.E., Lindsay, J.B., 2015. Characterizing ephemeral streams in a southern Ontario watershed using electrical resistance sensors. Hydrol. Process. 29 (1), 103–111.
Pekel, J.-F., Cottam, A., Gorelick, N., Belward, A.S., 2016. High-resolution mapping of global surface water and its long-term changes. Nature 540 (7633), 418–422.
Peleg, N., Shamir, E., Georgakakos, K., Morin, E., 2015. A framework for assessing hydrological regime sensitivity to climate change in a convective rainfall environment: a case study of two medium-sized eastern Mediterranean catchments. Israel. Hydrology and Earth System Sciences 19 (1), 567–581.
Pierini, N.A., Vivoni, E.R., Robles-Morua, A., Scott, R.L., Nearing, M.A., 2014. Using observations and a distributed hydrologic model to explore runoff thresholds linked with mesquite encroachment in the Sonoran Desert. Water Resour. Res. 50 (10), 8191–8215.
Powers, D.M., 2020. Evaluation: from precision, recall and F-measure to ROC, informedness, markedness and correlation. arXiv preprint arXiv:2010.16061.
Puckridge, J., Walker, K., Costelloe, J., 2000. Hydrological persistence and the ecology of dryland rivers. Regulated Rivers: Research & Management: An International Journal Devoted to River Research and Management 16 (5), 385–402.
Shaw, S.B., 2016. Investigating the linkage between streamflow recession rates and channel network contraction in a mesoscale catchment in New York state. Hydrol. Process. 30 (3), 479–492.
Shaw, S.B., Bonville, D.B., Chandler, D.G., 2017. Combining observations of channel network contraction and spatial discharge variation to inform spatial controls on baseflow in Birch Creek, Catskill Mountains, USA. J. Hydrol.: Reg. Stud. 12, 1–12.
Singh, V.P., 1997. Kinematic wave modeling in water resources: Environmental hydrology. John Wiley & Sons.
Smith, M.B., et al., 2004. The distributed model intercomparison project (DMIP): motivation and experiment design. J. Hydrol. 298 (1–4), 4–26.
Tian, F., Li, H., Sivapalan, M., 2012. Model diagnostic analysis of seasonal switching of runoff generation mechanisms in the Blue River basin, Oklahoma. J. Hydrol. 418, 136–149.
Tzoraki, O., De Girolamo, A.-M., Gamvroudis, C., Skoulikidis, N., 2016. Assessing the flow alteration of temporary streams under current conditions and changing climate by Soil and Water Assessment Tool model. International Journal of River Basin Management 14 (1), 9–18.
Vander Vorste, R., Malard, F., Datry, T., 2016. Is drift the primary process promoting the resilience of river invertebrate communities? A manipulative field experiment in an intermittent alluvial river. Freshw. Biol. 61 (8), 1276–1292.
Verdin, J., Funk, C., Senay, G., Choularton, R., 2005. Climate science and famine early warning. Philosophical Transactions of the Royal Society B: Biological Sciences 360 (1463), 2155–2168.

Vergara, H., et al., 2016. Estimating a-priori kinematic wave model parameters based on regionalization for flash flood forecasting in the Conterminous United States. J. Hydrol. 541, 421–433.
Viola, F., Pumo, D., Noto, L., 2014. EHSM: A conceptual ecohydrological model for daily streamflow simulation. Hydrol. Process. 28 (9), 3361–3372.
Vrugt, J.A., Ter Braak, C.J., Gupta, H.V., Robinson, B.A., 2009. Equifinality of formal (DREAM) and informal (GLUE) Bayesian approaches in hydrologic modeling? Stoch. Env. Res. Risk Assess. 23 (7), 1011–1026.
Walker, K.F., Sheldon, F., Puckridge, J.T., 1995. A perspective on dryland river ecosystems. Regulated Rivers: Research & Management 11 (1), 85–104.
Wang, J., et al., 2011. The coupled routing and excess storage (CREST) distributed hydrological model. Hydrol. Sci. J. 56 (1), 84–98.
Whiting, J.A., Godsey, S.E., 2016. Discontinuous headwater stream networks with stable flowheads, Salmon River basin. Idaho. Hydrological Processes 30 (13), 2305–2316.
Xue, X., et al., 2013. Statistical and hydrological evaluation of TRMM-based Multi-satellite Precipitation Analysis over the Wangchu Basin of Bhutan: Are the latest satellite precipitation products 3B42V7 ready for use in ungauged basins? J. Hydrol. 499, 91–99.
Ye, W., Bates, B., Viney, N., Sivapalan, M., Jakeman, A., 1997. Performance of conceptual rainfall-runoff models in low-yielding ephemeral catchments. Water Resour. Res. 33 (1), 153–166.
Zhang, J., et al., 2016. Multi-Radar Multi-Sensor (MRMS) quantitative precipitation estimation: Initial operating capabilities. Bull. Am. Meteorol. Soc. 97 (4), 621–638.
Zhang, Y., et al., 2015. Hydrometeorological analysis and remote sensing of extremes: Was the July 2012 Beijing flood event detectable and predictable by global satellite observing and global weather modeling systems? J. Hydrometeorol. 16 (1), 381–395.
Zhao, R., 1995. The xinanjiang model. Computer models of watershed hydrology 215–232.
Zimmer, M.A., McGlynn, B.L., 2017. Ephemeral and intermittent runoff generation processes in a low relief, highly weathered catchment. Water Resour. Res. 53 (8), 7055–7077.